Macromolecular Symposia

www.ms-journal.de

Synthesis, Characterization, and Photocatalytic Activity of NiO Nanoflowers

*Pradnya M. Bodhankar, Sapna Jadhav, and Pradip B. Sarawade**

The sustainable development of pollution-free technologies for environmental remediation has concerned significant attraction due to rapid growth of industrialization. Herein, synthesis of nanoflower-like NiO porous nanostructures prepared from different nickel precursors by solvothermal method in combination with calcination treatment is reported. The obtained porous NiO-Ac (prepared from nickel acetate) and NiO-S (prepared from nickel sulfate) nanostructures are analyzed by a powder X-ray diffractometer (XRD), transmission electron microscope (TEM), and BET to determine their structure, morphology, and surface area. Photocatalytic measurement of NiO-Ac and NiO-S demonstrates that, these nanostructures show excellent photo degradation behavior toward methylene blue (MB) under ultraviolet radiation. About 85% of MB in 100 min is removed using NiO-S nanostructured catalyst. Compared with NiO-Ac, the porous NiO-S nanoflowers exhibit higher photocatalytic activity due to their large surface area (100.79 $m^2 g^{-1}$) and smaller band gap (3.0 eV).

1. Introduction

Recently, water pollution by dye releases from different industries such as cosmetics, food processing, textile dyeing, paper making, etc, has drawn serious consideration due to hazards to epidemiology and environs.[1] The sacked wastes incorporating dyes are harmful to microorganisms, aquatic life, and human beings.[2] The discharge of the colored wastewaters in the environment is a substantial cause of non-aesthetic pollution and eutrophication and can emerge unhealthy outgrowth via oxidation, hydrolysis, or other chemical reactions taking place in the wastewater state. It ought to be referred to that dyes can present poisonous outcomes and decrease light penetration in contaminated waters.[3] Degradation of dyes in industrial wastewaters has consequently received growing interest and a few strategies of remediation has been proffered. Conventional physical approaches such as adsorption on activated carbon, ultrafiltration, reverse osmosis, coagulation by chemical agents, ion exchange on synthetic adsorbent resins, etc., were used for the elimination of dye pollutants.[4,5]

Recent research has been dedicated to the use of photocatalysis in the deportation of dyes from wastewaters, particularly, because of the proficiency of this technique to effectively mineralize the target pollutants. Photocatalysis can provide a simple and efficient approach to activate degradation of organic pollutants.[6–8] Accordingly, it is imperative to construct the different photocatalysts to improve the photocatalytic efficiency. According to the previous reports, nickel oxide's particle size, morphology, and crystalline phase are pretended to regulate its physicochemical properties.[9] With the aim to enhance the photocatalytic activity of nickel oxide nanostructures, it is great importance to synthesize well-defined nanostructures with unique morphology. It is widely accepted that, nickel oxide morphology highly influence the efficiency of the photo-catalysis process.[10] In earlier reports, Arshad et al. investigated NiO nanoflakes grafted graphene for photocatalytic degradation.[11] Martha's group fabricated NiO nanoparticles by thermal decomposition and evaluated degradation efficiencies at different annealing temperatures.[12] However, most of the reported procedures are complicated and the degradation efficiency is not high.[12,13]

In this work, we successfully prepared NiO nanoflowers with different nickel precursors using a simple solvothermal method. The composition, morphology, microstructure, and specific surface area were characterized via X-ray diffraction (XRD), transmission electron microscopy (TEM), and BET N_2 adsorption-desorption. The annealed products are used as the photocatalysts to degrade methylene blue (MB) dye.

2. Result and Discussion

2.1. Surface Morphology and Textural Properties of NiO

The surface morphologies of NiO catalysts were investigated by TEM, as presented in **Figure 1**. As can be seen from the TEM

P. M. Bodhankar, P. B. Sarawade
National Centre for Nanosciences and Nanotechnology
University of Mumbai
Vidyanagari, Santakruz (E), Mumbai, Maharashtra 400098, India
E-mail: pradnyadeshpande2000@gmail.com

P. M. Bodhankar, S. Jadhav, P. B. Sarawade
Department of Physics
University of Mumbai
Vidyanagari, Santakruz (E), Mumbai, Maharashtra 400098, India

S. Jadhav
SDSM College
University of Mumbai
Palghar 401404, India

The ORCID identification number(s) for the author(s) of this article can be found under https://doi.org/10.1002/masy.202100144

DOI: 10.1002/masy.202100144

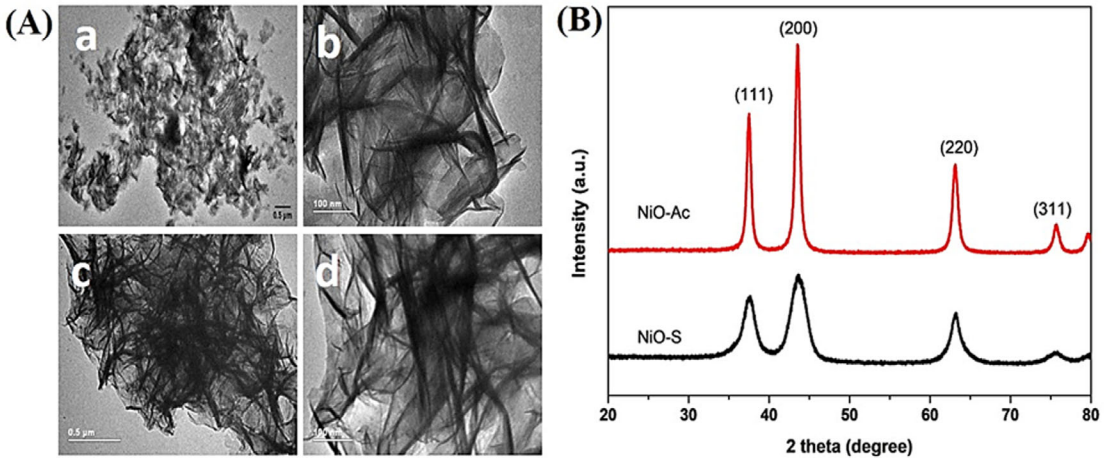

Figure 1. A) Low and high magnification TEM images of NiO-Ac (a and b); NiO-S (c and d), respectively. B) X-ray diffraction patterns of NiO-Ac and NiO-S, respectively.

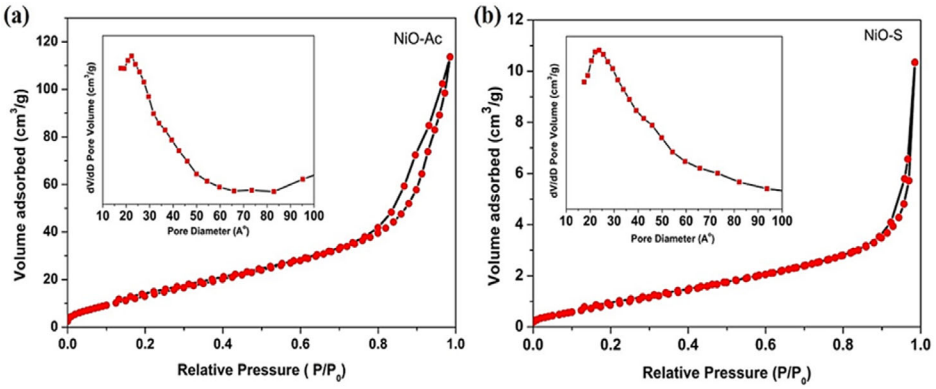

Figure 2. N_2 adsorption-desorption isotherms of NiO-Ac (a) and NiO-S (b), respectively; insets: Pore-size distribution for NiO-Ac (a) and NiO-S (b), respectively.

images (Figure 1Aa), NiO-Ac reflects a loose porous nanoflower-like structure, with sizes of 200–300 nm which are assembled from ultrathin nanosheets. Further, Figure 1Ab confirms the presence of ultrathin nanosheets in the NiO-Ac sample with a typical thickness of 4–6 nm. On the other hand, the NiO-S displayed a similar morphology (Figure 1Ac) to that of the NiO-Ac sample, except that the nanosheets of NiO-S are slightly thicker (8 nm) due to aggregation (Figure 1Ad).

The X-ray diffraction patterns of NiO-Ac and NiO-S nanostructures (Figure 1B) show peaks indexed to the pure phase of FCC NiO (JCPDS file No. 78-0643).[14] The peaks observed at of 37.48°, 43.6°, 63.18°, 75.72°, and 79.76° in both the NiO samples correspond to the (111), (200), (220), (311), and (222) planes. It can be seen from Figure 1B that the diffraction peaks in NiO-S sample are low and broad due to the small size effect. The XRD pattern shows that the samples are single phase and no other impurities distinct diffraction peaks except the characteristic peaks of FCC phase NiO was detected. This result shows that the physical phases of the NiO-Ac and NiO-S nanostructures have higher purity prepared in this work. The NiO lattice constant calculated from the XRD data is 4.177 Å, which is in good agreement with the reported data (JCPDS, No. 78-0643).[14] The average crystallite size is calculated by X-ray diffraction line broadening using the Scherrer formula $d = K\lambda/\beta \cos\theta$.[15] The crystallite sizes of NiO-Ac and NiO-S samples is 11.70 and 4 nm, respectively which was calculated from measured values for the spacing of the (200) plane.

Brunaur-Emmett-Teller (BET) analysis was performed for NiO-AC and NiO-S nanostructured samples to examine their surface areas. **Figure 2** shows the nitrogen (N_2) adsorption-desorption isotherms and BJH pore size distributions (PSDs) of the NiO-Ac and NiO-S nanostructures (Figure 2 (inset)). As shown in Figure 2A, the isotherm of the sample NiO-Ac is classified as type IV with H1 loop according to IUPAC classification, which is typical of mesoporous materials. The appearance of the H1 loop, which is often reported for materials consisting of agglomerates, indicates that the sample NiO-Ac has relatively high pore size uniformity and facile pore connectivity. This is in agreement with its TEM images (Figure 1Aa,Ab) and proven by its PSD data calculated using the desorption curve in the context of the BJH method. As shown in Figure 2A inset, the PDS histogram is narrow, which mainly cumulates at 20–25 Å with an average value of 22 Å. The BET surface areas of the NiO-Ac and NiO-S nanostructured catalysts were measured to be 59.76

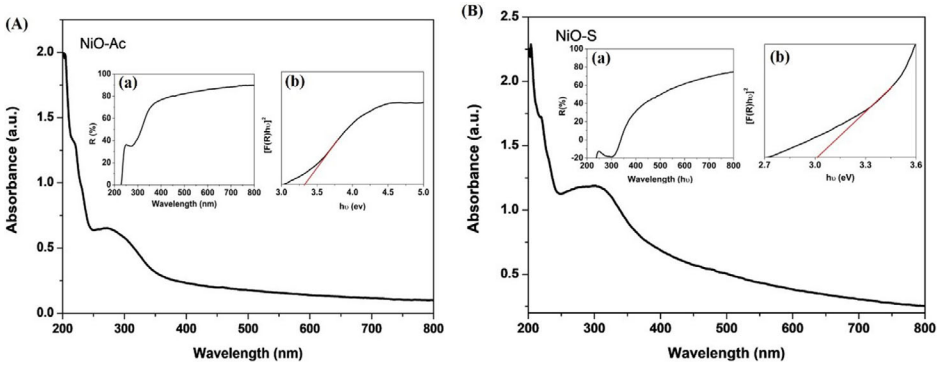

Figure 3. Absorption spectra of NiO-Ac (A) and NiO-S (B), respectively. Inset of (A): Diffuse reflectance spectra for NiO-Ac (a) and Kubelka-Munk transformed reflectance spectra NiO-Ac (b), respectively. Inset of (B): Diffuse reflectance spectra for NiO-S (a) and Kubelka-Munk transformed reflectance spectra NiO-S (b), respectively.

and 100.79 m^2 g^{-1}, respectively. Remarkable hysteresis of type IV was observed for nanostructured NiO-S, displayed by the BET adsorption-desorption isotherms (Figure 2B). This could be due to the capillary condensation of the adsorbed layer in NiO-S sample, also indicating mesoporous structures in the nanostructured NiO-S.

2.2. Optical Properties of NiO

The optical properties of NiO-Ac and NiO-S nanostructures were measured by UV-vis spectroscopy in diffuse reflectance (DR) mode. The absorption spectra were taken in the range of 200–800 nm as shown in **Figure 3**A,B. The results indicate that the maximum absorption peaks of the nanostructured NiO-Ac and NiO-S were identified at 257 and 294 nm, respectively. DR spectra of NiO-Ac and NiO-S are measured and presented in inset of Figure 3Aa,Ba, respectively. The DR spectra of the prepared samples after Kubelka-Munk treatment are shown in insets of Figure 3Ab,Bb. The band gap E_g of the prepared samples was extracted from the equation:

$$[F(R)\,h\upsilon]^2 = C\left(h\upsilon - E_g\right) \tag{1}$$

where C is absorption constant.[16] The energy band gap of the obtained NiO-Ac and NiO-S nanostructures is determined to be 3.3 and 3.0 eV, respectively. The optical band gap (Figure 3A,B (insets)) of both the nanostructures (NiO-Ac and NiO-S) in the present study is lower than the bulk value (3.65 eV). It is observed that the band gap of NiO-S is found to be less than NiO-Ac nanostructures as particle size is reduced from 11.7 to 4.0 nm. The size reduction causes large surface area to volume ratio, which in turn helps timely utilization of photo-generated carriers in interfacial processes.[17]

2.3. Photocatalytic Activity Results

For investigation of the photocatalytic activity of the prepared NiO samples, changes in the optical property of MB dye in an aqueous solution in the presence of NiO-Ac and NiO-S nanostructures under xenon lamp irradiation were measured. To reduce the environmental pollution caused due to these dyes, it is of great importance to decompose these dye molecules into some simple molecules. For evaluation of photocatalytic activities, 30 mg L^{-1} of MB dye solution was considered. In addition, optical properties of the NiO samples were measured using UV-vis-NIR spectrometer. The adsorption intensity deviation in MB dye adsorption spectra at wavelength of 644 nm was determined to evaluate the concentration change. First, pure MB dye without catalytic addition was assumed as reference under xenon lamp irradiation. Slight decomposition was observed after 160 min of illumination (**Figure 4**A).

Only below 6% of MB dye was decomposed under xenon lamp illumination in the absence of photocatalyst, meaning that MB dye self-degradation is negligible. However, substantial decrease in the MB dye concentration was observed after addition of the photocatalysts. Photocatalytic activation happens when light source photon energy is larger than or equal to the nickel oxide band gap energy. Equation (2) calculates MB dye degradation percentage,

$$\text{Degradation } \% = \frac{A_0 - A_t}{A_t} \times 100 \tag{2}$$

where, A_0 and A_t are the absorbance value of solution at 0 min and t min, respectively. Clearly, a strong relationship exists between the optical characteristics of the metal nanostructures and their shapes. Here, the maximum decomposition in MB solution concentration is observed when the nanostructured NiO-S was added, which is maybe due to their large surface area and small grain size to absorb a significant portion of UV irradiation. Using the NiO-S nanostructures, over 85% of MB dye degradation was obtained within 100 min light irradiation. The photocatalytic particles which are smaller in size involve further active surface sites and reveal more efficiency in surface charge carrier transfer. Resultantly, the number of surface-active sites increases, and thus MB dye degradation rate considerably enhances. Following equations (Equations 3–6) and schematic of dye degradation mechanism (Figure 4B) suggests the possible mechanism involved in the degradation of MB dye. In brief, the excitation of the positively charged holes from valence band to the conduction band occurs when NiO nanostructures are irradiated by the visible light (Equation 3). The superoxide anion

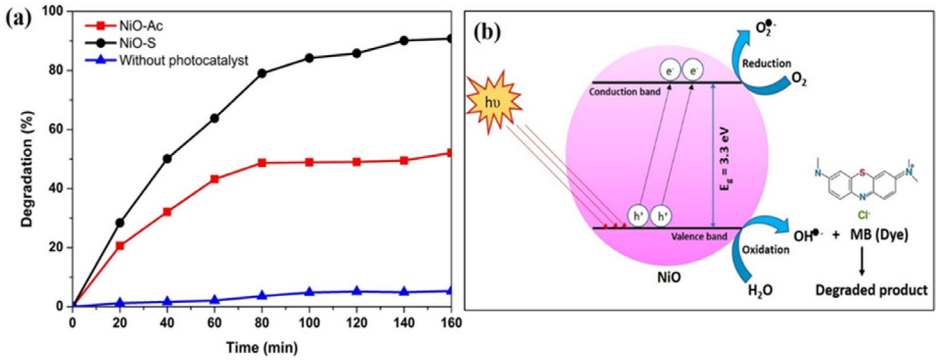

Figure 4. a) Photocatalytic efficiency of the MB dye degradation percentage curves by NiO-Ac and NiO-S, respectively. b) Schematic of photocatalytic degradation mechanism.

Table 1. Grain size, specific surface area, and energy band gap values.

Catalysts	FWHM [$d\theta$]	Grain size [nm]	BET surface area [$m^2\ g^{-1}$]	Energy band-gap [eV]
NiO-Ac	0.768	11.70	59.76	3.3
NiO-S	2.235	4.00	100.79	3.0

radicals are produced when electrons react with atmospheric oxygen (Equation 4). Meanwhile, holes react with water molecules to produce the hydroxyl radicals (Equation 5). These radicals are primarily responsible for the attacking MB dye molecules, which is adsorbed to the surface of NiO nanostructures.[18]

$$NiO + h\upsilon \rightarrow NiO\ \left(e^{-}_{CB} + h^{+}_{VB}\right) \quad (3)$$

$$e^{-}_{CB} + O_2 \rightarrow O_2^{\cdot -} \quad (4)$$

$$h^{+}_{VB} + H_2O \rightarrow OH^{\cdot} + H^{+} \quad (5)$$

$$MB\ (Dye) + O_2^{\cdot -} + OH^{\cdot} \rightarrow CO_2 + H_2O + \cdots \quad (6)$$

It is widely known that the catalytic process is mostly associated with the adsorption and molecular desorption on the catalytic surface. The high surface area NiO-S nanostructures allow for a comparatively rapid MB molecular diffusion and adsorb more incident light through multiple-reflections. Accordingly, the photocatalytic properties of different NiO nanostructures are different. It is, thus, expected that these NiO nanostructures show further promising physicochemical properties **Table 1**.

3. Conclusion

Nanostructured NiO have been successfully synthesized by different nickel precursors via facile solvothermal method. For morphological investigation of these structures, TEM analysis was applied. It was found that, the prepared nanostructures were fully crystalline and excellent monodispersed. The NiO-S showed the best photocatalytic MB dye degradation (85% in a time of ≈100 min). Compared to NiO-Ac, the prepared NiO-S gives a better photocatalytic performance due to high surface area and smaller band gap. Hence, further studies into the kinetics and fine-tuning of the low-cost and sustainable catalyst are in progress and shall be reported in future.

4. Experimental Section

Materials: All materials used in the synthesis and photocatalytic testing were of analytical grade and were purchased from Sigma Aldrich and used as received without further purification.

Synthesis of Nanoflower-Like NiO: The synthesis of NiO-Ac and NiO-S nanostructures had followed the reported method.[19] To synthesize the nanostructured form of NiO-Ac and NiO-S, the solvothermal route was adopted by using nickel (II) acetate tetrahydrate ($Ni(OCOCH_3)_2 4H_2O$) and nickel (II) sulfate hexahydrate ($NiSO_4\ 6H_2O$) as precursors, respectively. In a typical synthesis procedure, 0.66 M of urea ($CO(NH)_2$) and 0.20 M of cetyltrimethylammonium bromide ($CH_3(CH_2)15N(CH_3)_3Br$) (CTAB) were dissolved in 35 mL of cyclohexane (C_6H_{12}). The Nickel-based precursors, consisting of 0.177 m $Ni(OCOCH_3)_2\ 4H_2O$ and $NiSO_4\ 6H_2O$, respectively, were independently dissolved in 35 mL distilled water. The aqueous nickel precursor solution was then added to the cyclohexane mixture. The prepared homogeneous mixture was then poured into a 100 mL autoclave vessel (Teflon-lined) and heated in a hot-air oven at 120°C for 4 h. After the completion of the reaction, the solid products were formed depending on the nickel precursor. After washing these solid products were then dried in the air in an oven (60°C, 8 h) followed by annealing at 450°C in air to obtain the final NiO phase. The catalysts prepared from $Ni(OCOCH_3)_2\ 4H_2O$ and $NiSO_4.\ 6H_2O$ were denoted as NiO-Ac and NiO-S, respectively, and used for further characterization and investigation of their photocatalytic dye degradation performance.

Characterizations: For the morphological study, the microstructures of the catalysts were captured by transmission electron microscopy (TEM, JEM 2100, 200kV). The X-ray diffractometer (Rigaku Ultima IV, Cu-kα radiation) was employed to characterize the crystallinity and phase of the catalyst. The N_2 adsorption-desorption isotherms and physical surface areas were obtained by a Brunauer-Emmett-Teller (BET) surface area analyzer (Micromeritics ASAP 2000). Prior to the N_2 adsorption analysis, the catalyst powders were degassed under vacuum at a temperature of 120°C for 12 h. UV-vis absorption spectrometry measurements were carried out on a UV-vis-NIR absorption spectrophotometer (Cary) in diffuse reflectance mode in the range of 200–800 nm using ethanol as a reference solvent.

The photocatalytic activity of NiO-Ac and NiO-S nanostructured samples was evaluated by photo-degradation of MB under 150 W xenon lamp having spectrum similar to the solar spectrum. A total of 10 mg of similar photocatalysts were dispersed in 50 mL of aqueous MB (10 ppm). Prior to light irradiation, the solution was stirred for 30 min in dark so that the catalyst achieves adsorption equilibrium with MB. The distance between the light source and the reactor was kept constant at 45 cm. After fixed intervals of time, 1 mL of aqueous solution was filtered out in a 1 x 1 cm^2 cuvette. The normalized intensity of the absorption band of MB at

644 nm was measured and plotted as a function of irradiation time. All the photocatalytic experiments were done at room temperature and at neutral pH.

Acknowledgements

This work is financially supported by DST–WOS-A Scheme (SR/WOS-A/PM-9/2018(G)) and SERB (EEQ/2020/0002980) grants from Department of Science and Technology (DST), Govt. of India.

Conflict of Interest

The authors declare no conflict of interest.

Data Availability Statement

The data that support the findings of this study are available on request from the corresponding author. The data are not publicly available due to privacy or ethical restrictions.

Keywords

dye degradation, nanoflowers, nanostructures, photocatalyst

Received: April 15, 2021
Revised: May 18, 2021

[1] S. Hussain, N. Khan, S. Gul, S. Khan, H. Khan, *Water Chemistry*, IntechOpen, **2019**.
[2] P. Borker, A. Salker, *Mater. Sci. Eng., B* **2006**, *133*, 55.
[3] A. G. Prado, L. B. Bolzon, C. P. Pedroso, A. O. Moura, L. L. Costa, *Appl. Catal., B* **2008**, *82*, 219.
[4] I. K. Konstantinou, T. A. Albanis, *Appl. Catal., B* **2004**, *49*, 1.
[5] W. Z. Tang, H. An, *Chemosphere* **1995**, *31*, 4157.
[6] X.-J. Wen, C.-G. Niu, L. Zhang, C. Liang, G.-M. Zeng, *Appl. Catal., B* **2018**, *221*, 701.
[7] M. Iqbal, A. Ali, N. A. Nahyoon, A. Majeed, R. Pothu, S. Phulpoto, K. H. Thebo, *Mater. Sci. Energy Technol.* **2019**, *2*, 41.
[8] S. Gautam, H. Agrawal, M. Thakur, A. Akbari, H. Sharda, R. Kaur, M. Amini, *J. Environ. Chem. Eng.* **2020**, *8*, 103726.
[9] b. Anandan, V. Rajendran, *Mater. Sci. Semicond. Process.* **2011**, *14*, 43.
[10] Z. Qing, L. Haixia, L. Huali, L. Yu, Z. Huayong, L. Tianduo, *Appl. Surf. Sci.* **2015**, *328*, 525.
[11] A. Arshad, J. Iqbal, Q. Mansoor, *Nanoscale* **2017**, *9*, 16321.
[12] M. Ramesh, M. P. C. Rao, S. Anandan, H. Nagaraja, *J. Mater. Res.* **2018**, *33*, 601.
[13] S. D. Khairnar, V. S. Shrivastava, *J. Taibah. Univ. Sci.* **2019**, *13*, 1108.
[14] Z. Zhu, N. Wei, H. Liu, Z. He, *Adv. Powder Technol.* **2011**, *22*, 422.
[15] H. Qiao, Z. Wei, H. Yang, L. Zhu, X. Yan, *J. Nanomater.* **2009**, *2009*, 1.
[16] R. López, R. Gómez, *J. Sol-Gel Sci. Technol.* **2012**, *61*, 1.
[17] C.-m. Mo, L. Zhang, G. Wang, *Nanostruct. Mater.* **1995**, *6*, 823.
[18] A. J. Christy, M. Umadevi, *Mater. Res. Bull.* **2013**, *48*, 4248.
[19] P. M. Bodhankar, A. Chunduri, N. Patel, D. S. Dhawale, A. Vinu, H. Aljohani, P. B. Sarawade, *Sustain. Energy Fuels* **2021**, *5*, 1120.